Broadside Coupled Strip Inset Dielectric Guide and its Directional Coupler Application

Z. Fan and S. R. Pennock

Abstract—**A theoretical and numerical method is presented for the analysis of broadside-coupled strip inset dielectric guide. The method of analysis is based on an integral equation formulation and Galerkin's procedure. Besides propagation constants for two fundamental and higher order modes, the characteristic impedances for the two fundamental modes are calculated using the total propagating power and the longitudinal strip currents. The propagation characteristics of the two fundamental modes are then used to compute 4-port circuit parameters that are essential for accurate analysis and design of coupled line circuits. The effects of various structural parameters on the S-parameters are investigated and it is found that this broadside coupled strip IDG structure is useful for the realization of the directional couplers. Examples of strong and weak directional couplers are given. Furthermore, the propagation constants and S-parameters of coaxially excited coupled strips are measured, and are in good agreement with the theoretical analysis.**

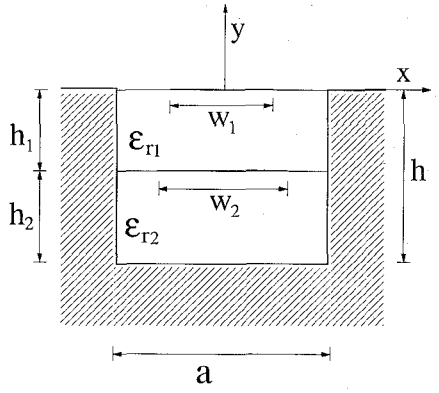

Fig. 1. Cross-section of a broadside coupled strip inset dielectric guide and the coordinate system used in the analysis.

I. Introduction

THE inset dielectric guide (IDG) has been proposed [1] as an alternative to image line. IDG has demonstrated advantages in terms of confinement of the electromagnetic field, low radiation loss at bends, possible ease of fabrication by use of plastic molding and spray metallization techniques, and inclusion of devices such as diodes with little performance degradation [2]. It has been also shown [3] that the twin layer IDG with high permittivity layer at the top of the groove exhibits very wide monomode bandwidth exceeding that of double ridge waveguide. In addition, the IDG can be integrated with other planar structures such as microstrip line [4]. This can be used for feeding planar antennas or as a low loss transmission line. In the latter case the propagation of surface modes, which can affect the performance of microstrip line, is prevented by the side walls of the groove.

The effective dielectric constant method [5] was first used to analyze the IDG structure. The transverse resonance diffraction (TRD) technique was then applied to IDG, and by considering the field singular boundary condition at the 90° metal edges, accurate results were obtained for the propagation constants of the first few modes and Q-factors [1]. The TRD method has also been extended to analyze the propagation characteristics of microstrip loaded IDG, embedded strip IDG and broadside coupled strip IDG structures [4], [6]–[9]. Published data for broadside coupled strip IDG are limited to the propagation constants of the two fundamental modes only. However, the propagation constants of the higher order modes should be determined to find the frequency range where only two fundamental modes propagate. Furthermore, a knowledge of the characteristic impedances of two fundamental modes is required if circuits, such as couplers, filters and antennas, are to be designed using broadside coupled strip IDG. This paper presents a rigorous method for calculating propagation constants and characteristic impedances of the broadside coupled strip IDG, and hence, the 4-port parameters of its equivalent circuit.

Manuscript received April 5, 1993; revised July 12, 1994.

The authors are with the School of Electronic and Electrical Engineering, University of Bath, Claverton Down, Bath, BA2 7AY, U.K.

IEEE Log Number 9407471.

II. Formulation of Integral Equations

Fig. 1 shows the cross section of broadside-coupled strip inset dielectric guide and the coordinate system used in the analysis. An $\exp j(wt-\beta z)$ time and z dependence is assumed for all field and current quantities. Electromagnetic field components in the slot region can be represented through their discrete Fourier transforms:

$$E_y(x,y) = \frac{1}{a}\sum_{n=-\infty}^{\infty} \tilde{E}_y(\alpha_n, y)e^{-j\alpha_n x} \tag{1}$$

and similarly for other field components. To satisfy the electric field boundary conditions at the sidewalls of the slot, the values of α_n are constrained to be $\alpha_n = 2n\pi/a$ for the E_z odd modes, $\alpha_n = ((2n+1)\pi)/a$ for the E_z even modes including two fundamental modes, where $n = 0, \pm 1, \pm 2, \ldots$.

Since the air region is unbounded in x, field components in the air region are expressed in terms of continuous Fourier transforms, for example:

$$E_y(x,y) = \frac{1}{2\pi}\int_{-\infty}^{\infty} \tilde{E}_y(\alpha, y)e^{-j\alpha x}d\alpha. \tag{2}$$

Solutions to the wave equations in the Fourier transformed domain are obtained for the different regions of the structure (air, upper and lower dielectric layers in the slot). The solutions contain coefficients determined by applying the boundary conditions at infinity, on the base of the slot and across the lower interface and introducing the electric field components transverse to y at the upper interface. Enforcing the conditions that the current density components at $y = 0$ vanish for $w_1/2 < |x| < a/2$ and that the tangential electric field components at $y = -h_1$ vanish for $|x| < w_2/2$ leads to four integral equations for tangential electric field components at $y = 0$ and current components at $y = -h_1$.

$$\frac{1}{2\pi}\int_{-\infty}^{\infty}[Y_{i1}^{a}\tilde{E}_x^u(\alpha)+Y_{i2}^{a}\tilde{E}_z^u(\alpha)]e^{-j\alpha x}d\alpha+\frac{1}{a}\sum_{n=-\infty}^{\infty}\times[Y_{i1}^{s}\tilde{E}_x^u(\alpha_n)+Y_{i2}^{s}\tilde{E}_z^u(\alpha_n)+Y_{i3}^{s}\tilde{J}_x^l(\alpha_n)+Y_{i4}^{s}\tilde{J}_z^l(\alpha_n)]\times e^{-j\alpha_n x}=0 \quad \text{for } \frac{w_1}{2}<|x|<\frac{a}{2} \quad i=1,2 \tag{3}$$

$$\frac{1}{a}\sum_{n=-\infty}^{\infty}[Y_{i1}^{s}\tilde{E}_x^u(\alpha_n)+Y_{i2}^{s}\tilde{E}_z^u(\alpha_n)+Y_{i3}^{s}\tilde{J}_x^l(\alpha_n)+Y_{i4}^{s}\tilde{J}_z^l(\alpha_n)]e^{-j\alpha_n x}=0 \quad \text{for } |x|<\frac{w_2}{2} \quad i=3,4. \tag{4}$$

III. Application of Galerkin's Method

In order to solve integral equations (3)–(4), Galerkin's method is applied. Expanding electric field components at $y = 0$ and current components at $y = -h_1$ in terms of known basis functions and taking the inner product of the integral equations with basis functions yield a homogeneous matrix equation for the unknown expansion coefficients.

$$\begin{bmatrix} K_{im}^{a11}+K_{im}^{s11} & K_{im}^{a12}+K_{im}^{s12} & K_{im}^{s13} & K_{im}^{s14} \\ K_{im}^{a21}+K_{im}^{s21} & K_{im}^{a22}+K_{im}^{s22} & K_{im}^{s23} & K_{im}^{s24} \\ K_{im}^{s31} & K_{im}^{s32} & K_{im}^{s33} & K_{im}^{s34} \\ K_{im}^{s41} & K_{im}^{s42} & K_{im}^{s43} & K_{im}^{s44} \end{bmatrix}\begin{bmatrix} C_{xm}^{E} \\ C_{zm}^{E} \\ C_{xm}^{J} \\ C_{zm}^{J} \end{bmatrix}=0. \tag{5}$$

The elements of the matrix $[K]$ are given by

$$K_{im}^{shp}=\frac{1}{a}\sum_{n=-\infty}^{\infty}K_i^{sh}(-\alpha_n)Y_{hp}^{s}K_m^{sp}(\alpha_n) \quad h,p=1,2,3,4 \tag{6}$$

$$K_{im}^{ahp}=\frac{1}{2\pi}\int_{n=-\infty}^{\infty}K_i^{ah}(-\alpha_n)Y_{hp}^{a}K_m^{ap}(\alpha)d\alpha \quad h,p=1,2 \tag{7}$$

where

$$K_m^{s1}(\alpha_n)=\tilde{E}_{xm}^u(\alpha_n), \quad K_m^{s2}(\alpha_n)=\tilde{E}_{zm}^u(\alpha_n)$$
$$K_m^{s3}(\alpha_n)=\tilde{J}_{xm}^l(\alpha_n), \quad K_m^{s4}(\alpha_n)=\tilde{J}_{zm}^l(\alpha_n)$$
$$K_m^{a1}(\alpha)=\tilde{E}_{xm}^u(\alpha), \quad K_m^{a2}(\alpha)=\tilde{E}_{zm}^u(\alpha)$$

and

$$\tilde{E}_{xm}^u(\alpha_n)=\left(\int_{-\frac{a}{2}}^{-\frac{w_1}{2}}+\int_{\frac{w_1}{2}}^{\frac{a}{2}}\right)E_{xm}^u(x)e^{j\alpha_n x}\,dx \tag{8}$$

$$\tilde{E}_{zm}^u(\alpha_n)=\left(\int_{-\frac{a}{2}}^{-\frac{w_1}{2}}+\int_{\frac{w_1}{2}}^{\frac{a}{2}}\right)E_{zm}^u(x)e^{j\alpha_n x}\,dx \tag{9}$$

$$\tilde{J}_{xm}^l(\alpha_n)=\int_{-\frac{w_2}{2}}^{\frac{w_2}{2}}J_{xm}^l(x)e^{j\alpha_n x}\,dx \tag{10}$$

$$\tilde{J}_{zm}^l(\alpha_n)=\int_{-\frac{w_2}{2}}^{\frac{w_2}{2}}J_{zm}^l(x)e^{j\alpha_n x}\,dx. \tag{11}$$

For nontrivial solutions for C_{xm}^E, C_{zm}^E, C_{xm}^J and C_{zm}^J, the determinant of the coefficient matrix in (5) must be zero. This condition results in the determinantal equation for the propagation constant.

$$\text{Det}\,[K_{im}]=0. \tag{12}$$

To evaluate the matrix elements in (12), the Fourier transforms of the basis functions in (8)–(11) must be first computed. Integrating (9) and (10) by parts and considering the boundary conditions that require that z electric field component must be zero at conducting edges on the upper surface and x current component on the lower strip must be zero at the edges of the lower strip, the following expressions for $\tilde{E}_{zm}^u(\alpha_n)$ and $\tilde{J}_{xm}^l(\alpha_n)$ are obtained

$$\tilde{E}_{zm}^u(\alpha_n)=\frac{j}{\alpha_n}\left(\int_{-\frac{a}{2}}^{-\frac{w_1}{2}}+\int_{\frac{w_1}{2}}^{\frac{a}{2}}\right)\frac{\partial E_{zm}^u(x)}{\partial x}e^{j\alpha_n x}\,dx \tag{13}$$

$$\tilde{J}_{xm}^l(\alpha_n)=\frac{j}{\alpha_n}\int_{-\frac{w_2}{2}}^{\frac{w_2}{2}}\frac{\partial J_{xm}^l(x)}{\partial x}e^{j\alpha_n x}\,dx. \tag{14}$$

As $(\partial E_z^u(x))/\partial x$ and $(\partial J_x^l(x))/\partial x$ satisfy the same boundary and singular edge conditions as $E_x^u(x)$ and $J_z^l(x)$ respectively, the basis functions $(\partial E_{zm}^u(x))/\partial x$ and $(\partial J_{xm}^l(x))/\partial x$ can be chosen to be the same as $E_{xm}^u(x)$ and $J_{zm}^l(x)$ respectively. Furthermore, the convergence in computing the matrix elements in (6) and (7) is improved because the factor j/α_n appears in (13) and (14).

To achieve fast convergence of the solutions of the determinantal equation, the edge conditions satisfied by tangential electric field components on the upper interface and current components on the lower strip should be accounted for in the choice of basis functions. Due to the presence of the metallic corners at $x = \pm a/2$ and the edges of the upper conducting strip at $x = \pm w_1/2$, the electric field is singular at the corners and the edges. It can be shown [4] that E_x^u and $\partial E_z^u/\partial x$ have the same singular behavior of type $r^{-\frac{1}{3}}$ at metallic corners and of type $r^{-\frac{1}{2}}$ at the edges of the strip. To include this singular behavior in the basis function, the following basis functions E_{xm}^u and $\partial E_{zm}^u/\partial x$ are chosen

$$E_{xm}^u(x)=\frac{\partial E_{zm}^u(x)}{\partial x}=\frac{1}{N_m^P}(1-x')^{-\frac{1}{3}}(1+x')^{-\frac{1}{2}}\begin{cases}P_m^{(-\frac{1}{3},-\frac{1}{2})}(x') \text{ for } \frac{w_1}{2}<x<\frac{a}{2}\\ \pm P_m^{(-\frac{1}{3},-\frac{1}{2})}(x') \text{ for } -\frac{a}{2}<x<-\frac{w_1}{2}\end{cases} \tag{15}$$

where $x' = 2(|x| - x_0)/w_s$, $x_0 = (a + w_1)/4$ and $w_s = (a - w_1)/2$. $P_m^{(-\frac{1}{3},-\frac{1}{2})}$ are Jacobi polynomials, and N_m^P are normalization factors. The plus and minus signs in $\pm$ are

chosen for the E_z odd and even modes, respectively. It should be noted that for E^u_{xm} the series starts at 0, but for $\partial E^u_{zm}/\partial x$ the series starts at 1. The reason for this is twofold. a) E^u_z is zero at the strip edge ($x = w_1/2$) and the metallic corner ($x = a/2$) so that $\partial E^u_z/\partial x$ must have zero average in the range. b) $\int_{\frac{w_1}{2}}^{\frac{a}{2}} (\partial E^u_{z0}(x)/\partial x)dx \neq 0$.

Similarly, the presence of the edges of the lower conducting strip at $x = \pm w_2/2$ introduces singularities in the current distribution. The singularity is of type $r^{-\frac{1}{2}}$ at the strip edges. Taking the edge singularity into account, the basis functions $\partial J^l_{xm}/\partial x$ and J^l_{zm} are chosen as follows

$$\frac{\partial J^l_{xm}(x)}{\partial x} = J^l_{zm}(x) = \frac{1}{N^T_n}\left[1 - \left(\frac{2x}{w_2}\right)^2\right]^{-\frac{1}{2}} \times T_n\left(\frac{2x}{w_2}\right) \text{ for } |x| < \frac{w_2}{2} \tag{16}$$

where T_n are Chebyshev polynomials, and N^T_n are normalization factors. $n = 2m + 1$ and $n = 2m$ are chosen for the E_z odd and even modes, respectively. Note that $m = 0, 1, 2, \cdots$ except that $m = 1, 2, \cdots$ for $\partial J^l_{xm}/\partial x$ for the E_z even mode since the zeroth term of $J_x(x)$ for the E_z even mode is not zero at the edges of the lower strip as boundary conditions require.

IV. Characteristic Impedances

As there are two conducting strips in the IDG structure, there are two modes that propagate at all frequencies, the two fundamental modes. At low enough frequencies the longitudinal components of electric and magnetic field are negligible compared to the corresponding transverse field components, and so these two modes can be called quasi-TEM modes. To obtain an equivalent coupled line circuit for the structure considered here, which is useful for the analysis and design of coupled-strip circuits such as directional couplers, the characteristic impedances of these two modes must be first determined. However, for the quasi-TEM structure, unique definition does not exist due to the existence of longitudinal field components (specially at higher frequencies). For the microstrip-like or other quasi-TEM structures, the most commonly used impedance definition is that based on the total transported power and the currents on the strips.

Once the propagation constants of two fundamental modes, β_1 and β_2 are found, the total power flow P_j along the guide for each mode and total longitudinal currents I_{ij} on each conducting strip for each mode can be evaluated, where $i = 1$ for the lower strip, 2 for the upper strip and $j = 1$ for mode 1, 2 for mode 2. The voltage V_{ij} at strip i due to mode j can be found by using the definition of modal power and the reciprocity theorem [10].

$$P_j = \frac{1}{2}\int_s \vec{E}_j \times \vec{H}^*_j \cdot d\vec{s} = \frac{1}{2}\sum_{k=1}^{2} V_{kj} I^*_{kj} \quad (j = 1, 2) \tag{17}$$

$$\frac{1}{2}\int_s \vec{E}_i \times \vec{H}_j \cdot ds = \frac{1}{2}\sum_{k=1}^{2} V_{ki} I_{kj} = 0 \quad (i, j = 1, 2; i \neq j). \tag{18}$$

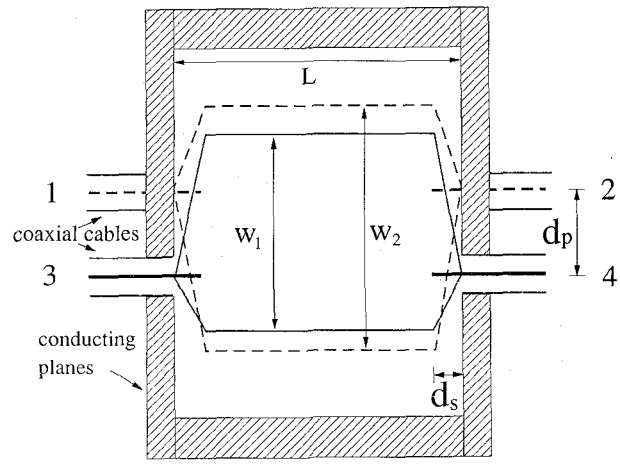

Fig. 2. Top view of the experimental structure for measurements of S-parameters.

A characteristic impedance Z_{ij} of strip i for mode j is

$$Z_{ij} = \frac{V_{ij}}{I_{ij}}. \tag{19}$$

The following relations can be found for the lossless structure.

$$\frac{Z_{11}}{Z_{21}} = \frac{Z_{12}}{Z_{22}} = -R^i_1 R^i_2, \quad \frac{V_{21}}{V_{11}} = -\frac{1}{R^i_2}\frac{V_{22}}{V_{12}} = -\frac{1}{R^i_1} \tag{20}$$

where R^i_j is current ratio for mode j, given by $R^i_j = I_{2j}/I_{1j}$

For a certain frequency range only the two fundamental modes propagate. In this range the characteristics of these two modes can be used to design a directional coupler where the coupling occurs in the backward direction. Once the propagation constants, characteristic impedances and strip current ratios of the two fundamental modes are found, the impedance matrix $[Z]$ of a length L of broadside coupled strip IDG can be calculated using the expressions in [11]. Scattering matrix can be obtained from the impedance matrix using the following relation $[S] = ([Z] - Z_0[I])([Z] + Z_0[I])^{-1}$, where $[I]$ is the unit matrix and Z_0 represents the normalizing impedance at each port. The ports of the 4-port coupler are defined in Fig. 2.

V. Numerical Results

Numerical results showed that two or three basis functions for each expansion quantity are sufficient to obtain accurate solutions for propagation constants to four significant digits. More basis functions are required to obtain accurate solutions for the characteristic impedances. The characteristic impedances are stable to less than 0.5% using six basis functions for each expansion quantity.

Fig. 3 shows the dispersion characteristics of the first few even and odd modes up to 10 GHz. In this structure there is no symmetry plane between the coupled strips. The terms even and odd refer to the only symmetry plane in this structure, the plane through both strips at $x = 0$. The figure shows that the

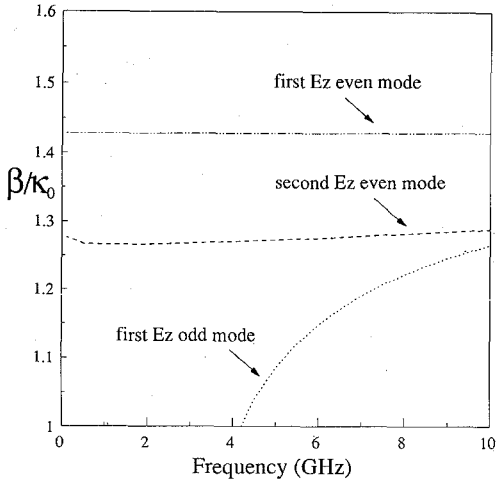

Fig. 3. Dispersion characteristics of the first few even and odd modes (a = 10.16 mm, h_1 = 2.54 mm, h_2 = 12.7 mm, $\varepsilon_{r1} = \varepsilon_{r2}$ = 2.04, w_1 = 7.0 mm, and w_2 = 5.0 mm).

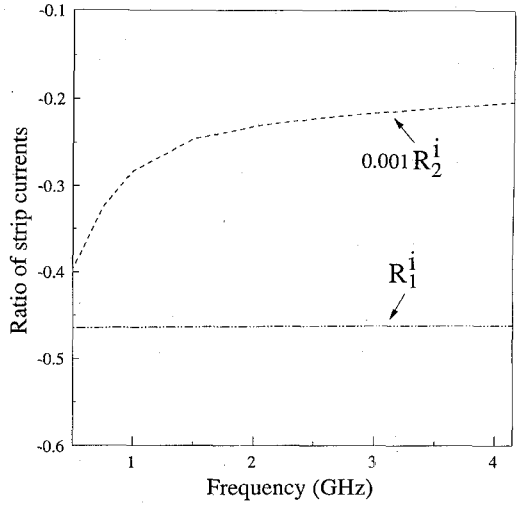

Fig. 4. Frequency dispersion of strip current ratios of two fundamental modes for ε_{r1} = 2.04 (a = 10.16 mm, h_1 = 2.54 mm, h_2 = 12.7 mm, ε_{r2} = 2.04, w_1 = 7.0 mm, and w_2 = 5.0 mm).

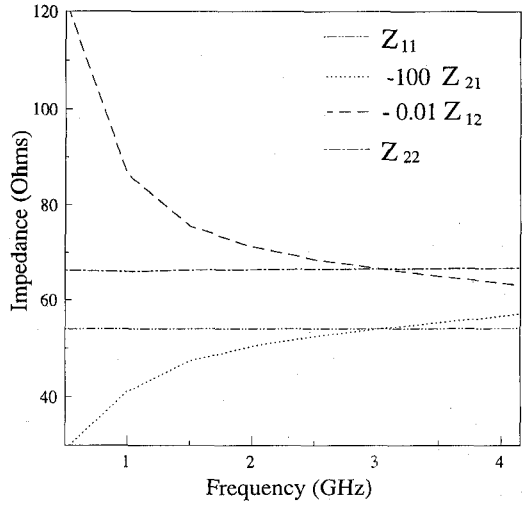

Fig. 5. Frequency dispersion of characteristic impedances of two fundamental modes for ε_{r1} = 2.04 (a = 10.16 mm, h_1 = 2.54 mm, h_2 = 12.7 mm, ε_{r2} = 2.04,w_1 = 7.0 mm, and w_2 = 5.0 mm).

two fundamental modes are the first two E_z even modes, and the first higher order mode is an odd E_z mode.

Figs. 4 and 5 shows the frequency dependence of strip current ratios and characteristic impedances of two fundamental modes for $\varepsilon_{r1} = 42.0$, respectively. It can be seen that Z_{11} and Z_{22} change very little as frequency increases. Values of Z_{21} and Z_{12} are negative and change as frequency increases. As can be seen from the relation for the characteristic impedances in the previous section, the reason for this is that the values of R_1^i and R_2^i are negative. At very low frequency the results for characteristic impedance obtained here by using the total power and strip currents, are the same as those obtained by using the strip currents and voltages on the two strips. These voltages are determined by integrating the electric field from the strips to the IDG conducting surfaces. It has been also found that R_1^i is always negative and its absolute value increases as ε_{r1} increases. In addition R_2^i is negative for small value of ε_{r1}, but positive for large value of ε_{r1} and $1/R_2^i$ increases as ε_{r1} increases. As a result, for higher values of ε_{r1}, R_1^i is negative and R_2^i is positive, and thus, the values of Z_{21} and Z_{12} become positive. This can be observed from Figs. 6 and 7 which show frequency dependence of strip current ratios and characteristic impedances of two fundamental modes for $\varepsilon_{r1} = 4.7$, respectively.

The S-parameters S_{11}, S_{21}, S_{31} and S_{41} are shown in Fig. 8 as a function of frequency. Clearly port 4 is the isolated port, and the reflection coefficient S_{11} is small. As is expected, the coupler is a backward coupler, with coupling to port 3. It is also observed that the maximum coupling (S_{31}) from port 1 to port 3 is obtained when $(\beta_1 + \beta_2)l = \pi$, at 2 GHz in this example. Fig. 9 shows the S-parameters as a function of the width of the upper strip. It can be observed that S_{41} is the most greatly affected by the change of w_1. There exists a minimum value of S_{41} (maximum isolation) at a certain value of w_1. Fig. 10 shows S-parameters as a function of the width of the lower strip. As w_2 increases, S_{21} and S_{31} change very little, but S_{11} and S_{41} change rapidly. There is an optimum value for minimum reflection coefficient, but there is also a different optimum value of w_2 for maximum isolation. Fig. 11 shows the S-parameters as a function of the thickness of the upper substrate. It can be found that coupling S_{31} increases as h_1 decreases and S_{41} is always smaller than S_{31}. Hence the change of h_1 enables both tight and loose coupling values to be achieved. With the appropriate choices of values of w_1 and w_2 minimum reflection coefficient and maximum isolation can be obtained. Therefore, the broadside coupled strip IDG structure can realize both high and low coupling value directional couplers with good input match and high directivity.

VI. Experimental Verification

To assess the accuracy of the analysis presented in previous sections, measured results have been obtained for comparison with computed results. Propagation constants were measured using the resonant section method [3]. This method can measure the propagation constants of the E_z even and odd modes independently by changing the orientation of the magnetic probes. These probes are inserted at the line center over the

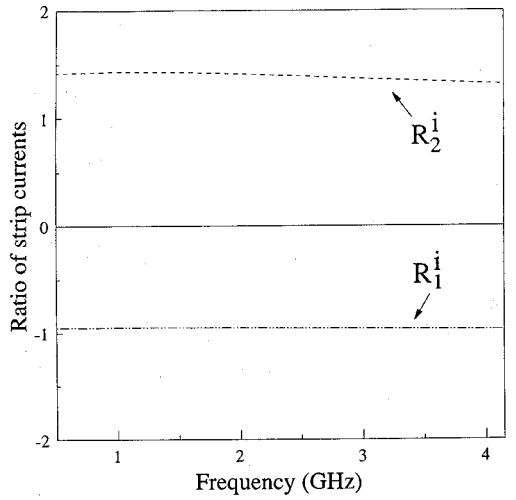

Fig. 6. Frequency dispersion of strip current ratios of two fundamental modes for $\varepsilon_{r1} = 4.7$ ($a = 10.16$ mm, $h_1 =$ mm, $h_2 = 12.7$ mm, $\varepsilon_{r2} = 2.04$, $w_1 = 7.0$ mm and $w_2 = 5.0$ mm).

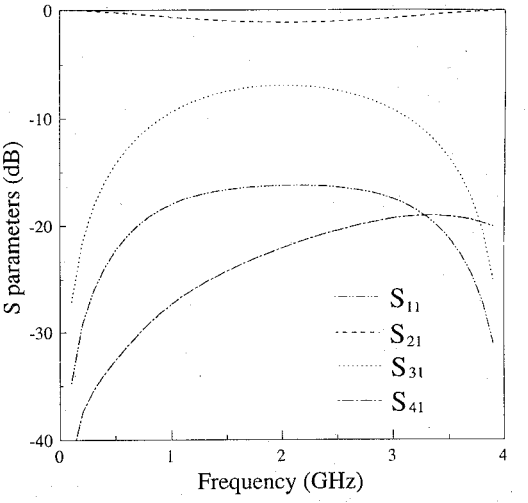

Fig. 8. S-parameters as a function of frequency ($a = 10.16$ mm, $h_1 = 2.54$ mm, $h_2 = 1.27$ mm, $\varepsilon_{r1} = \varepsilon_{r2} = 2.04$, $w_1 = 7.0$ mm, $w_2 = 5.0$ mm, $Z_0 = 50\ \Omega$, and $L = 27.8$ mm).

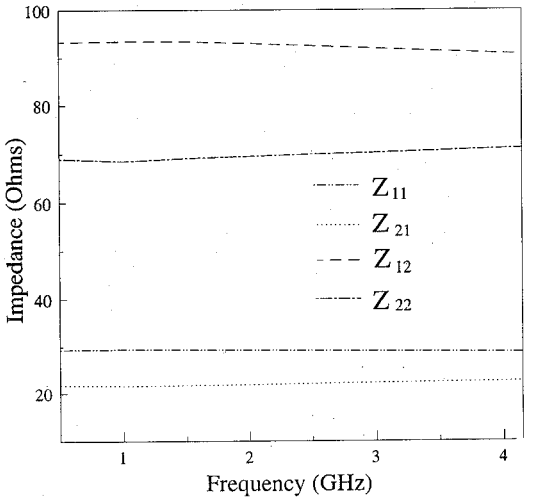

Fig. 7. Frequency dispersion of characteristic impedances of two fundamental modes for $\varepsilon_{r1} = 4.7$ ($a = 10.16$ mm, $h_1 = 2.54$ mm, $h_2 = 12.7$ mm, $\varepsilon_{r2} = 2.04$, $w_1 = 7.0$ mm, and $w_2 = 5.0$ mm).

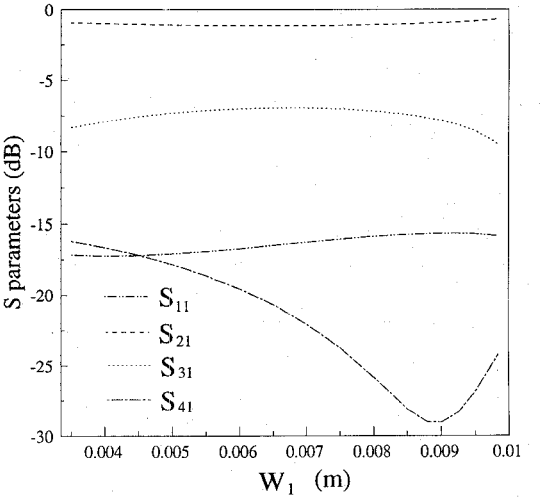

Fig. 9. S-parameters as a function of w_1 ($a = 10.16$ mm, $h_1 = 2.54$ mm, $h_2 = 1.27$ mm, $\varepsilon_{r1} = \varepsilon_{r2} = 2.04$, $w_2 = 5.0$ mm, $f = 2$ GHz, $Z_0 = 50\ \Omega$, and $L = \pi/(\beta_1 + \beta_2)$).

upper surface, through short circuit plates at both ends of the IDG section.

Comparison between measured and computed results for the propagation constants is shown in Fig. 12. The agreement between experiment and theory for the second E_z even mode and the first E_z odd mode is good—within 1%. No comparison for the first E_z even mode is presented as the positioning of the magnetic probes over the structure produces little excitation of this mode. The fields of the first E_z mode of this structure are concentrated in the region between the two strips. Comparison of the present results with calculated and measured results available in [7] is shown in Fig. 13 for the propagation constants of the first and second E_z even modes. Clearly the agreement between these data for two fundamental modes is good.

To assess the accuracy of the predicted S-parameters for a directional coupler the configuration in Fig. 2 was used. The dielectric used for both layers in the slot was PTFE. The 4-port coupler was excited using semi-rigid coaxial cables which were introduced through holes in the metal end plates, in the same manner as connection is generally made to microstrip circuits. The protruding central conductor of the coaxial cable was soldered to the strips in the IDG slot. The spacing between the coupled strips was quite small in some cases, and so the excitation points needed to be offset from the center of the slot, as shown in Fig. 2. To minimize discontinuity series inductance at the excitation points, short tapered ends to the conducting strips were used.

The S-parameters of the IDG coupler were measured using our HP8510B Network Analyzer. The Analyser was calibrated on 3.5 mm coaxial cable ports, and connected to the coupler ports i and j. The remaining coupler ports were terminated by coaxial matched loads. The input reflection and forward transmission coefficients for this arrangement can be measured

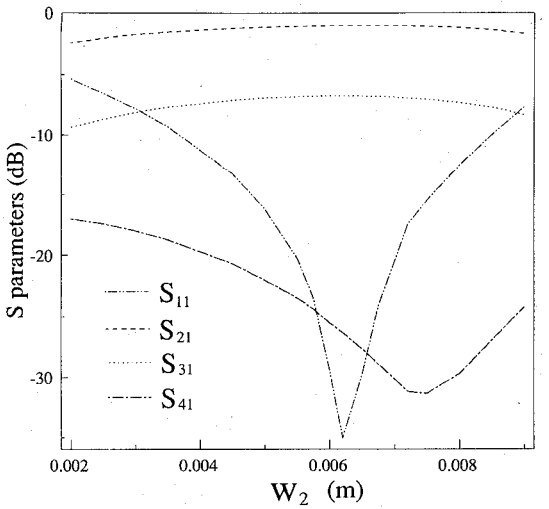

Fig. 10. S-parameters as a function of w_2 ($a = 10.16$ mm, $h_1 = 2.54$ mm, $h_2 = 12.7$ mm, $\varepsilon_{r1} = \varepsilon_{r2} = 2.04$, $w_1 = 7.0$ mm, $f = 2$ GHz, $Z_0 = 50$ Ω, and $L = \pi/(\beta_1 + \beta_2)$).

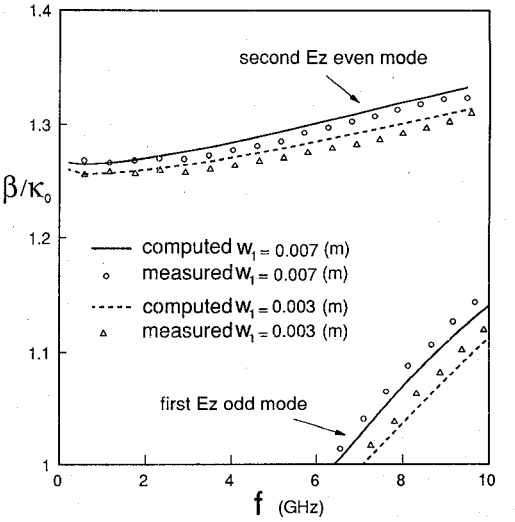

Fig. 12. Comparison of computed and measured propagation constants for the second E_z even mode and first E_z odd mode ($a = 22.86$ mm, $h_1 = 2.16$ mm, $h_2 = 8.0$ mm, $\varepsilon_{r1} = \varepsilon_{r2} = 2.04$, and $w_2 = w_1$).

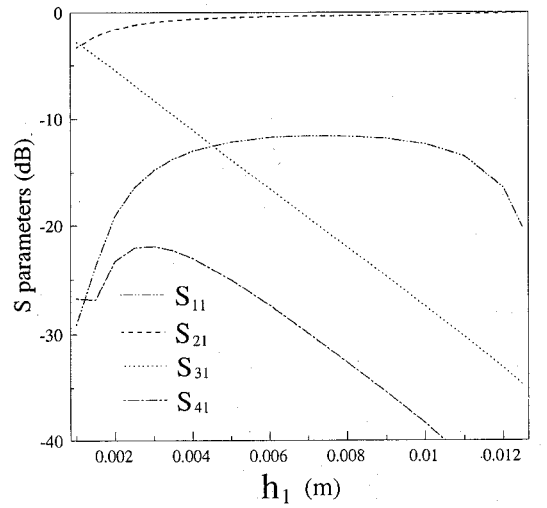

Fig. 11. S-parameters as a function of h_1 ($a = 10.16$ mm, $h = 4$ 15.2 mm, $\varepsilon_{r1} = \varepsilon_{r2} = 2.04$, $w_1 = 7.0$ mm, $w_2 = 5.0$ mm, $f = 2$ GHz, $Z_0 = 50$ Ω, and $L = \pi/(\beta_1 + \beta_2)$).

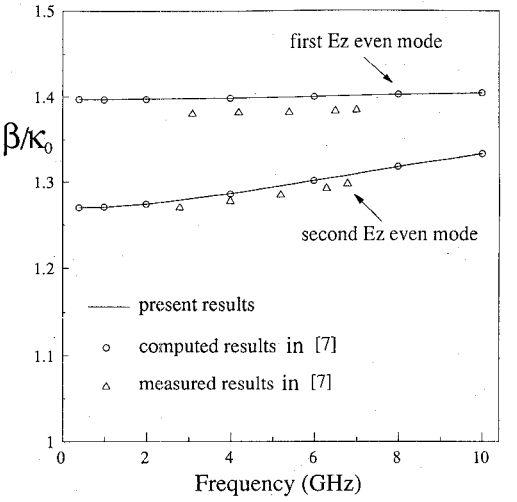

Fig. 13. Comparison of present computed propagation constants with computed and measured data obtained by Izzat in [7] for two fundamental modes ($a = 22.86$ mm, $h_1 = 2.16$ mm, $h_2 = 8.0$ mm, $\varepsilon_{r1} = \varepsilon_{r2} = 2.04$, $w_1 = 5.0$ mm, and $w_2 = 10.0$ mm).

and as a result measured S-parameters S_{ii}, S_{jj}, S_{ij} and S_{ji} of the coupler are obtained. Two coupler examples were used, showing strong and weak peak coupling. The structural parameters are given in the figures. Due to the symmetry of the structure there are only six independent S-parameters: S_{11}, S_{21}, S_{31}, S_{41}, S_{33} and S_{43}.

Figs. 14 and 15 show the comparison of the computed and measured S-parameters for Example 1. It is clearly seen that there is an excellent agreement between theory and experiment for the coupling S_{31}. There is little difference between the computed and measured S_{21} and S_{43}. There is also reasonable agreement between theory and experiment for the reflection coefficients S_{11} and S_{33} and isolation S_{41}. The computed and measured curves for S_{11}, S_{33} and S_{41} reach peaks at almost the same values of frequency and differences at most of these peaks are less than 2 dB. These discrepancies arise as the discontinuities between the IDG section and cables are not taken into account in the theoretical model. There may also be a small air gap between two layers of dielectric in the practical structure, and there is a tolerance of 1–2% in the permittivity of dielectric.

Figs. 16 and 17 show the comparison of the computed and measured S-parameters for Example 2. Again the good agreement between theory and experiment is obtained for all the S-parameters. It is noted that reflection coefficients from port 1 and port 3, S_{11} and S_{33}, are very different. This arose as the design of this coupler only considered input match at port 1. Furthermore, it is found that the maximum coupling for both samples occurs at frequencies where $(\beta_1 + \beta_2)l = \pi, 3.2\pi, 5.4\pi, 7.6\pi, \cdots$ and decreases slightly with frequency. The curves for S_{41} also reach peaks at different values of frequency. However with increasing frequency peak value for S_{41} increases very quickly and consequently the isolation becomes much worse. Therefore,

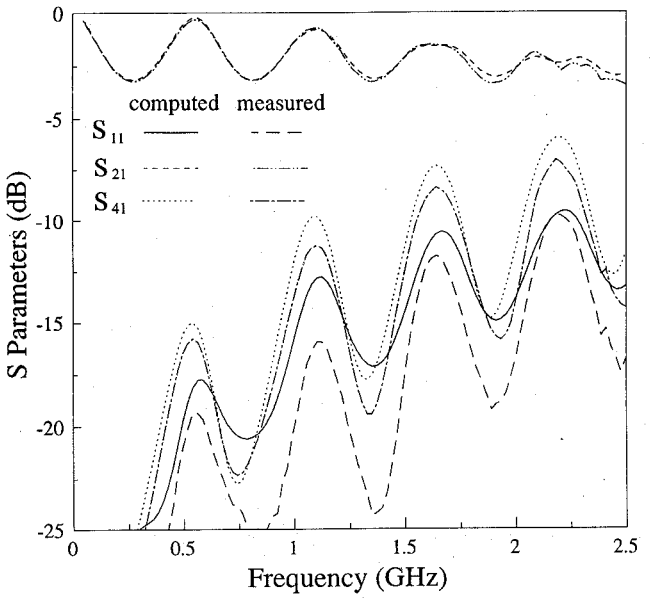

Fig. 14. Comparison of computed and measured S-parameters S_{11}, S_{21} and S_{41} of Example 1 ($\varepsilon_{r1} = 2.04$, $\varepsilon_{r2} = 2.04$, $a = 22.86$ mm, $h_1 = 2.16$ mm, $h_2 = 8.0$ mm, and $w_1 = w_2 = 10.0$ mm).

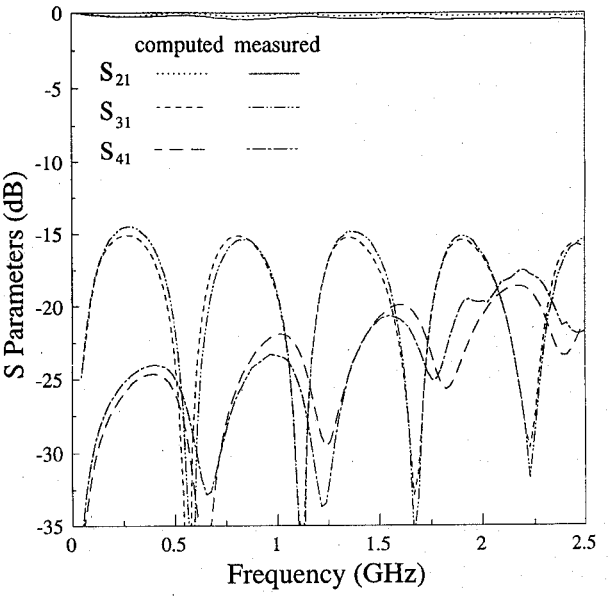

Fig. 16. Comparison of computed and measured S-parameters S_{21}, S_{31} and S_{41} of Example 2 ($\varepsilon_{r1} = 2.04$, $\varepsilon_{r2} = 2.04$, $a = 22.86$ mm, $h_1 = 8.0$ mm, $h_2 = 2.16$ mm, and $w_1 = w_2 = 7.0$ mm).

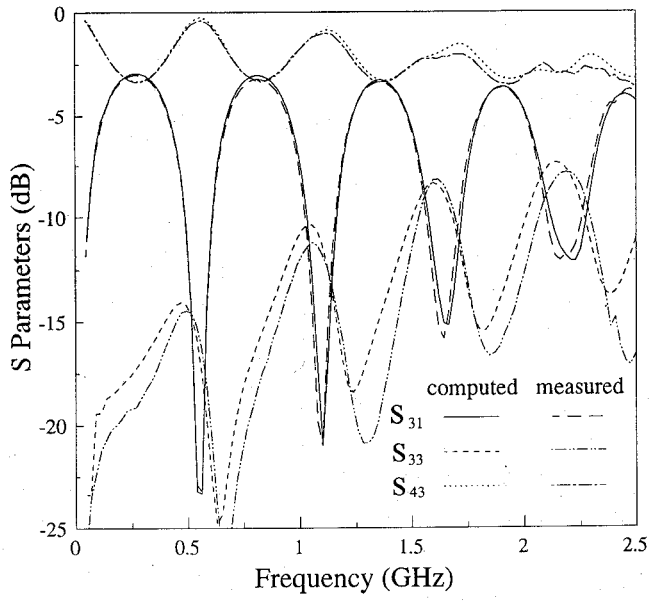

Fig. 15. Comparison of computed and measured S-parameters S_{31}, S_{33} and S_{43} of Example 1 ($\varepsilon_{r1} = 2.04$, $\varepsilon_{r2} = 2.04$, $a = 22.86$ mm, $h_1 = 2.16$ mm, $h_2 = 8.0$ mm, and $w_1 = w_2 = 10.0$ mm).

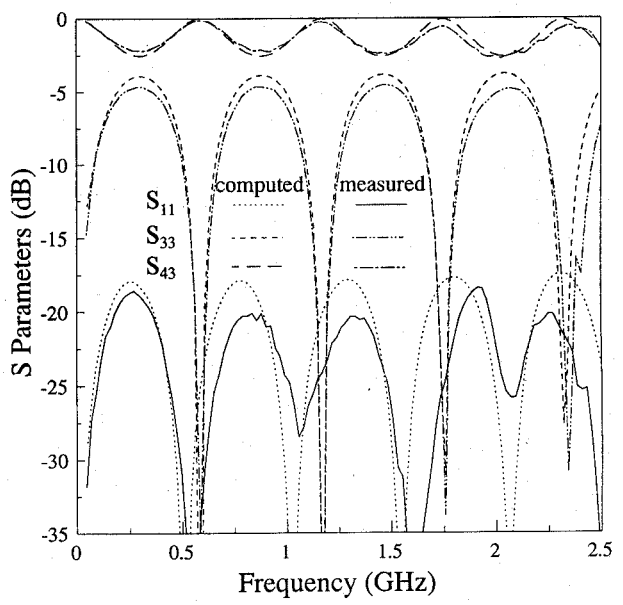

Fig. 17. Comparison of computed and measured S-parameters S_{11}, S_{33} and S_{43} of Example 2 ($\varepsilon_{r1} = 2.04$, $\varepsilon_{r2} = 2.04$, $a = 22.86$ mm, $h_1 = 8.0$ mm, $h_2 = 2.16$ mm, and $w_1 = w_2 = 7.0$ mm).

it is demonstrated theoretically and experimentally that for a high directivity coupler, the length of the IDG section should be chosen to be $\pi/(\beta_1 + \beta_2)$ at the center frequency.

VII. Conclusion

This paper presents a theoretical and numerical method for calculating propagation constants and characteristic impedances of broadside coupled strip IDG by means of an integral equation formulation and Galerkin's method. Numerical results for propagation constants and characteristic impedances have been presented and are in good agreement with measured results for propagation constants. The 4-port S-parameters of the coupled lines have been found from the propagation characteristics of the two fundamental modes. Numerical results for scattering parameters are presented for various values of structural parameters. It is found that both strong and weak directional couplers can be realized by using a section of this structure with appropriate choices of the distance between the strips and the widths of the strips.

Broadside coupled strip directional couplers have been realized, excited via coaxial cables, for both high and low peak coupling value couplers. Measured S-parameters obtained using a Network Analyzer are in good agreement with theoretical predictions.

APPENDIX

The quantities in (3) and (4) are given by

$$
\begin{aligned}
Y_{11}^s &= j(G_1\alpha_n^2 - G_4\beta^2)D^s,\\
Y_{12}^s &= Y_{21}^s = j\alpha_n\beta(G_1 + G_4)D^s\\
Y_{13}^s &= Y_{31}^s = (G_2\alpha_n^2 + G_5\beta^2)D^s\\
Y_{14}^s &= Y_{41}^s = Y_{23}^s = Y_{32}^s = \alpha_n\beta(G_2 - G_5)D^s\\
Y_{22}^s &= j(G_1\beta^2 - G_4\alpha_n^2)D^s,\\
Y_{24}^s &= Y_{42}^s = (G_2\beta^2 + G_5\alpha_n^2)D^s\\
Y_{33}^s &= j(G_3\alpha_n^2 - G_6\beta^2)D^s,\\
Y_{34}^s &= Y_{43}^s = j\alpha_n\beta(G_3 + G_6)D^s\\
Y_{44}^s &= j(G_3\beta^2 - G_6\alpha_n^2)D^s,\\
Y_{11}^a &= j\left(-\frac{\gamma_0}{w\mu_0}\beta^2 + \frac{w\varepsilon_0}{\gamma_0}\alpha^2\right)D^a\\
Y_{22}^a &= j\left(-\frac{\gamma_0}{w\mu_0}\alpha^2 + \frac{w\varepsilon_0}{\gamma_0}\beta^2\right)D^a,\\
Y_{12}^a &= Y_{21}^a = j\alpha\beta\left(\frac{\gamma_0}{w\mu_0} + \frac{w\varepsilon_0}{\gamma_0}\right)D^a
\end{aligned}
$$

where

$$
\begin{aligned}
G_1 &= \frac{1}{Q_e}w\varepsilon_0\varepsilon_{r1}(\gamma_2\varepsilon_{r1}\tanh\gamma_2h_2\tanh\gamma_1h_1 + \gamma_1\varepsilon_{r2})\\
G_2 &= \frac{1}{Q_e}\frac{\gamma_1\gamma_2\varepsilon_{r1}}{\cosh\gamma_1h_1}\tanh\gamma_2h_2\\
G_3 &= \frac{1}{Q_e}\frac{\gamma_1^2\gamma_2}{w\varepsilon_0}\tanh\gamma_1h_1\tanh\gamma_2h_2\\
G_4 &= \frac{1}{Q_h}\gamma_1(\gamma_2 + \gamma_1\tanh\gamma_1h_1\tanh\gamma_2h_2)\\
G_5 &= \frac{1}{Q_h}\frac{w\mu_0\gamma_1}{\cosh\gamma_1h_1}\tanh\gamma_2h_2\\
G_6 &= \frac{1}{Q_h}(w\mu_0)^2\tanh\gamma_2h_2\tanh\gamma_1h_1\\
Q_e &= \gamma_1(\gamma_2\varepsilon_{r1}\tanh\gamma_2h_2 + \gamma_1\varepsilon_{r2}\tanh\gamma_1h_1)\\
Q_h &= w\mu_0(\gamma_2\tanh\gamma_1h_1 + \gamma_1\tanh\gamma_2h_2)\\
D^s &= 1/(\alpha_n^2 + \beta^2), \quad D^a = 1/(\alpha^2 + \beta^2)\\
\gamma_i^2 &= \alpha_n^2 + \beta^2 - \kappa_0^2\varepsilon_{ri} \quad \text{for } i = 1,2;\gamma_0^2 = \alpha^2 + \beta^2 - \kappa_0^2\\
\kappa_0^2 &= w^2\mu_0\varepsilon_0.
\end{aligned}
$$

REFERENCES

[1] T. Rozzi and S. J. Hedges, "Rigorous analysis and network modeling of the inset dielectric guide," *IEEE Trans. Microwave Theory Tech.*, vol. MTT-35, pp. 823–833, Sept. 1987.

[2] S. R. Pennock, T. Rozzi, and A. DiFilippo, "Inset dielectric guide mounting of a detector diode," *IEEE Microwave and Guided Wave Lett.*, vol. 1, pp. 168–170, May 1992.

[3] S. R. Pennock, N. Izzat, and T. Rozzi, "Very wideband operation of twin-layer inset dielectric guide," *IEEE Trans. Microwave Theory Tech.*, vol. 40, pp. 1910–1917, Oct. 1992.

[4] T. Rozzi, A. Morini, and G. Gerini, "Analysis and applications of microstrip loaded inset dielectric waveguide," *IEEE Trans. Microwave Theory Tech.*, vol. 40, pp. 272–278, Feb. 1992.

[5] W. Zhou and T. Itoh, "Analysis of trapped image guides using effective dielectric constant and surface impedances," *IEEE Trans. Microwave Theory Tech.*, vol. MTT-30, pp. 2163–2166, Dec. 1982.

[6] T. Rozzi, G. Gerini, A. Morini, and M. Santis, "Multilayer buried microstrip inset guide," in *Proc. 21st European Microwave Conf.*, Stuttgart, 1991, pp. 673–678.

[7] N. Izzat, "Space domain analysis of inhomogeneous waveguides of the microstrip and inset guide families," Ph.D. dissertation, Bath University, Bath, 1991.

[8] Z. Fan and S. R. Pennock, "Analysis of broadside coupled strip inset dielectric guide," in *Proc. 1993 IEEE MTT-S Int. Microwave Symp.*, Atlanta, GA, June 1993, pp. 839–842.

[9] N. Izzat, S. R. Pennock, and T. Rozzi, "Space domain analysis of micro-IDG structures," *IEEE Trans. Microwave Theory Tech.*, vol. 42, June 1994.

[10] F. L. Mesa, G. Cano, F. Medina, R. Marques, and M. Horno, "On the quasi TEM and full wave approaches applied to coplanar multistrip on lossy dielectric layered media," *IEEE Trans. Microwave Theory Tech.*, vol. 40, pp. 524–532, Mar. 1992.

[11] V. K. Tripathi, "Asymmetric coupled transmission lines in an inhomogeneous medium," *IEEE Trans. Microwave Theory Tech.*, vol. MTT-23, pp. 734–739, 1975.

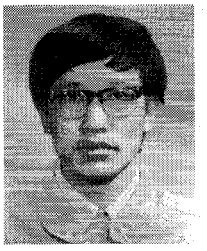

Z. Fan received the B.Sc. degree in physics from Hubei University in 1983, and the M.Sc degree in microwave and antennas from Wuhan University, P.R. China, in 1986. In 1994 he received the Ph.D. degree from the University of Bath, U.K., for his work on inset dielectric guide structures and ferrite loaded finlines.

From 1986 to 1991 he was a lecturer at Wuhan University. From 1991 to 1994 he was a postgraduate student at the University of Bath. His research interests are in the areas of novel waveguide structures, microstrip antennas, ferrite devices, and microwave circuits.

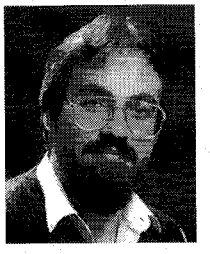

S. R. Pennock (M'88) was born in Birmingham, U.K., in 1959. He received the B.Sc. degree in physics with electronics from the University of Liverpool, U.K., in 1980 and the Ph.D. degree from the University of Bath, U.K., in 1986 for his work on the Plasmatic Control of Dielectric Waveguides.

From 1983 to 1985 he was a Research Assistant working on Finline Components for Millimeter Waves at the University of Bath, where, in 1985 he became a lecturer. His current research interests include the modeling of novel transmission lines, uniform and nonuniform transmission structures, antennas, active and control circuits, and measurements at microwave and millimeter wave frequencies.